Sub-6 GHz Energy Detection-based Fast On-Chip Analog Spectrum Sensing with Learning-driven

Signal Classification

Ankit Mittal, Graduate Student Member, IEEE, Milin Zhang, Graduate Student Member, IEEE, Thomas Gourousis, Graduate Student Member, IEEE, Ziyue Zhang, Graduate Student Member, IEEE, Yunsi Fei, Senior Member, IEEE, Marvin Onabajo, Senior Member, IEEE, Francesco Restuccia, Senior Member, IEEE, and Aatmesh Shrivastava, Senior Member, IEEE

Abstract—Cognitive communication utilizes transient openings in the spectrum to communicate opportunistically, which is a promising technique to enable more efficient spectrum usage in an increasingly congested spectrum environment. We aim to address two main challenges associated with cognitive communication: (i) spectrum sensing should be fast and energy efficient for processing a large bandwidth in a short time; (ii) the spectrum sensing approach should be able to simultaneously recognize multiple signals that are present. In this paper, we propose to address these challenges with a novel design framework that consists of a fast onchip spectrum sensing in conjunction with a novel learning-based spectrum analysis model at the edge to enhance the optimizations for spectrum agility. We first utilize a model of a programmable analog-based high-quality factor (Q) on-chip spectrum sensor that is capable of scanning the sub-6 GHz band to detect the spectrum usage in less than 1μ s. The proposed spectrum sensor also enhances the energy efficiency of the sensing. To complement the onchip spectrum sensor, a deep learning (DL) model is deployed for a fine-grained signal detection between channels in the 400 MHz to 6 GHz range, which is intended to be executed on edge devices. Simulation results show that the DL model can detect multiple different modulated signals with a mean Intersection-over-Union (IoU) of 86.8% in highly-variable bandwidth and center frequency scenarios. Finally, we present a system-level model of our framework to demonstrate the spectrum sensing and classification in the sub-6 GHz frequency band.

Index Terms—Spectrum sensing, cognitive radio, dynamic spectrum access (DSA), interference sensing, integrated sensing and communications.

I. INTRODUCTION

N unprecedented growth of Internet of Things (IoT) devices accessing the sub-6 GHz range to support various applications such as healthcare [1], [2], smart home [3], [4], and agriculture devices [5], [6] has rendered the spectrum exceptionally crowded.

An anticipated 50 billion IoT devices are expected to be absorbed into the spectrum by the year 2030 [7]. This would

A. Mittal, M. Zhang, T. Gourousis, Z. Zhang, Y. Fei, M. Onabajo, F. Restuccia and A. Shrivastava are with the Department of Electrical and Computer Engineering, Northeastern University, Boston, MA, 02115 USA. e-mail: ({mittal.ank, zhang.mil, gourousis.t, zhang.ziyue, y.fei}@northeastern.edu, monabajo@ece.neu.edu, f.restuccia@northeastern.edu, aatmesh@ece.neu.edu.)

This material is based upon work supported by the National Science Foundation under grant no. 2146754 and no. 2225368, and is supported in part by funds from OUSD R&E, NIST, and industry partners as specified in the Resilient & Intelligent NextG Systems (RINGS) program

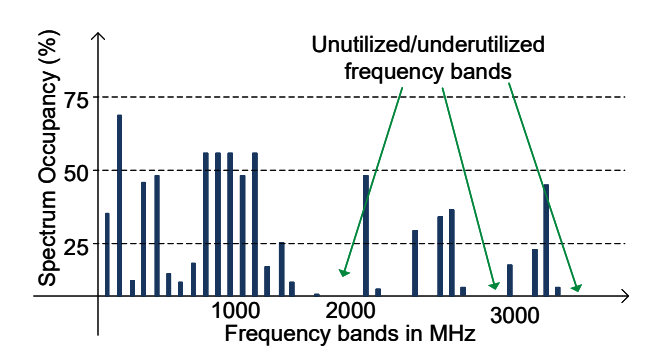


Fig. 1. Visualization of how the underused/underutilized sub-6 GHz spectrum offers opportunities for dynamic spectrum access.

further overwhelm the already resource-limited wireless spectrum. There is a compelling need to design radio networks that will handle such scale of congestion while assuring the desired quality of service (QoS). In [8], it is reported that there is a spatio-temporal under-utilization of the licensed bands that are otherwise reserved for incumbent users. Agile communication, which uses cognitive radio (CR), exploits this feature of the licensed bands to opportunistically access the band when the incumbent user is inactive, with hopping onto the next available band when the incumbent user is detected. Spectrum sensing is a key component of CR, which identifies spectral openings known as spectral opportunities to enable dynamic spectrum access (DSA). Fig. 1 exemplifies spectrum occupancy and visualizes the utilization of spectral bands, highlighting those that are either unused or underutilized.

Wideband spectrum sensing techniques are highly favorable over conventional narrow-band sensing techniques [9] on account of two main factors: (i) they offer a wider detection range, and (ii) at higher frequencies, the possibility of a higher channel throughput (Shannon's channel capacity). Several wideband spectrum sensing techniques reported in the literature [10]–[16] include sampling of the RF signals using a high-bandwidth analog-to-digital converter (ADC) followed by a digital fast Fourier transform (FFT) block [15]. Sub-Nyquist sampling techniques, which involve the sub-sampling of a sparse channel, have been employed to reduce the power consumption of Nyquist-based ADCs based on low sparsity with unknown sparsity basis. The assumption of sparsity, on which this sens-

1

ing is based, becomes less reliable in massive IoT networks where activity depends on spatial-temporal dynamics and time-varying fading channels [17]. These techniques involve a higher sensing time, high power consumption (100s of milliwatt) and associated higher computational costs, making them prohibitive for spectrum sensing with low-power IoT devices.

Energy detection-based techniques measure the power level of RF signals in the band of interest, and compare it with the expected noise power in the absence of RF signals [16]. Energy detection-based spectrum sensing is a promising solution as a cost effective technique, providing an ability to detect the spectral opportunities by analyzing the energy content in different sub-bands in the sensing bandwidth. It promises to be a suitable sensing technique for low-power IoT devices due to its high energy efficiency. However, limited detection range and performance under poor signal-to-noise ratio (SNR) have been major drawbacks that limit its adoption for DSA. Moreover, energy detection is a blind detection technique, implying that it is unable to differentiate between cognitive communication and the incumbent user. As a result, deep learning (DL) approaches are proposed to classify different signals in the spectrum [18]– [23] to enable more complex spectrum policies such that different wireless signals can have different priorities.

Although DL shows significant advantage in signal classification in low SNR [24] and dynamic path loss [25] scenarios, it operates only on the baseband signal and requires knowledge of the signal's carrier frequency for implementation. Such approaches intrinsically assume that both the transmitter and receiver operate at the same frequency. Conventional DL approaches typically take the entire spectrum data at the receiver's center frequency as input, resulting in a single label output for signal types. However, signals in the wideband spectrum may not always be centered around the receiver's frequency, and there may be multiple signals present simultaneously. Consequently, conventional DL algorithms are limited in providing detailed information about signal locations in the wideband spectrum. In essence, an effective wideband spectrum sensing approach requires addressing two critical aspects: determining the signal type and identifying its location in the spectrum. In this regard, conventional DL approaches are not well suited for blind detection in wideband scenarios. Very recently, computer vision based approaches were proposed to jointly determine the signal type and carrier frequency in a wide band [26], [27]. These works convert the wideband spectrum to images using signal processing approaches, such as the short-time Fourier transform, and apply object detection algorithms from computer vision applications such as YOLOv3 [28] directly to spectrum images. However, such vision-based approaches require pre-processing for converting the spectrum to images and post-processing such as non-maximum suppression to filter the detection, resulting in a large delay for computation [27].

To alleviate the above issues, we first propose a wideband energy detection-based spectrum sensor. This is implemented using analog-based spectrum sensor that detects the energy in the sub-6 GHz band using programmable high-quality factor (Q) filters. We use a differential topology to improve the accuracy of filtering with a sensing bandwidth of 40 MHz. Further, in contrast to vision-based signal classification methods, we

introduce an innovative approach, namely *semantic spectrum segmentation*, with a new deep neural network (DNN) architecture that directly operates on 1-dimensional waveform data of the spectrum without additional processing. As a result, it significantly reduces the computation resources as well as the inference latency. Furthermore, the proposed algorithm partitions the spectrum into multiple sub-channels in the frequency domain and assigns labels to each sub-channel based on the semantic features of the signal. In contrast to conventional DL-based approaches that cannot identify the location of signals, the classifier can jointly classify the type of multiple signals as well as localize them in the wideband spectrum without the prior knowledge of the carrier frequency, enabling a better optimization of spectrum policies [29].

The DL algorithm is introduced to complement the onchip spectrum sensor, providing fine-grained information of signals in 40 MHz band for real-time optimizations in agile IoT networks. We present a system design that combine the cost benefit of energy detection-based spectrum sensing together with our agile communication platform, which enables wideband sensing and signal feature identification for lowpower IoT networks. The proposed framework has the potential to be applied to a diverse range of applications such as in smartphones and wearable devices [30]–[33]. To the best of our knowledge, no prior work has reported the incorporation of onchip spectrum sensing and DL signal classification at the edge into CR.

The main contributions of this paper are as follows:

- It introduces an analog spectrum sensor architecture to perform fast spectrum scanning of the sub-6 GHz band in less than 1μ s.
- It proposes a DL algorithm for fine-grained spectrum analysis in sub-bands. The proposed DL model can jointly localize and classify signals by semantic segmentation without pre- or post-processing. Compared to existing work, the proposed approach is able to reduce the latency by 61.15% while having adequate classification performance.
- A combined agile simulation platform is presented to integrate analog spectrum sensing with DL-based signal classification.

The rest of the paper is organized as follows. Section II discusses the system architecture of the agile spectrum sensing and classification approach. Section III and IV provides the details of the on-chip spectrum sensor and the DL algorithm for edge devices respectively. In Section V, we describe a system model of the architecture in Simulink and present simulation results for the spectrum sensing, classification and authentication. Finally, conclusions are presented in Section VI.

II. SYSTEM ARCHITECTURE

Fig. 2 displays the proposed agile communication approach with multiple IoT nodes containing analog spectrum sensors and an edge device containing both, an analog spectrum sensor and a DNN classifier. On the IoT nodes side, the spectrum sensor will scan and perform energy detection in the sub-6 GHz band. This is achieved by a concurrent sensing in each channel

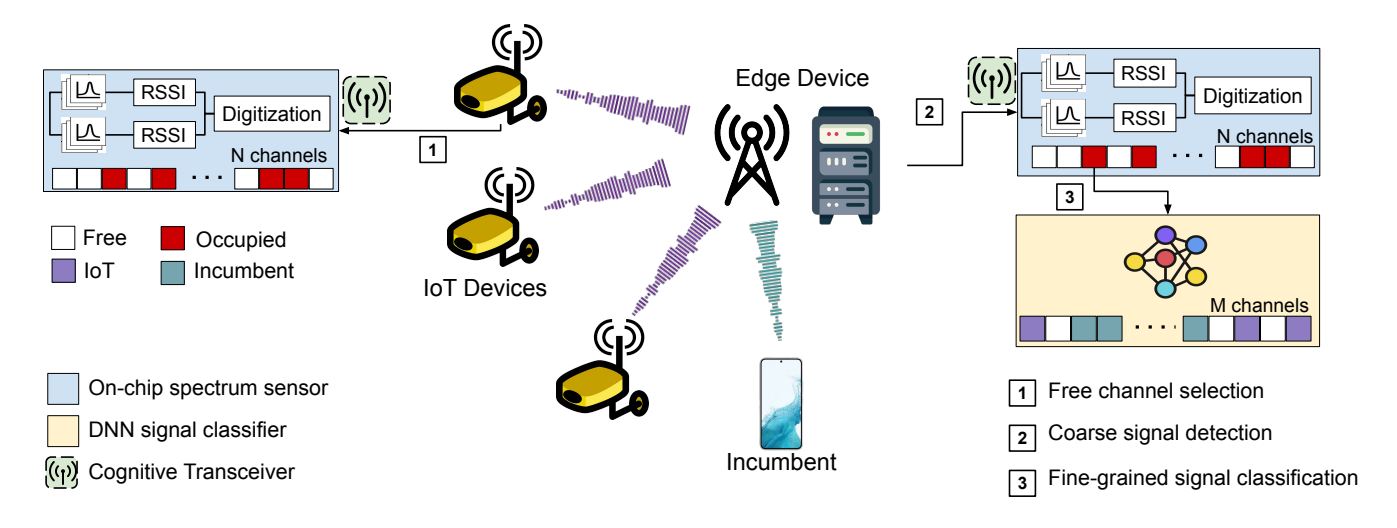


Fig. 2. Envisioned agile platform consisting of IoT devices equipped with energy detection-based analog spectrum sensors and an edge device with a spectrum sensor and a DNN signal classifier for intelligent identification.

of 40 MHz bandwidth (141 channels), which involves amplifying the signal content and processing it using the received signal strength indicator (RSSI) circuit in each 40 MHz window. Based on a specified signal energy detection threshold level, the spectrum sensor classifies the congestion state of the band. This fast spectrum sensing provides a coarse classification of the channel as a foundation of agile communication. The IoT cognitive radio then sends a request to the edge device for a connection in the identified minimally congested (free) band, and will wait a period of time for handshaking. The IoT cognitive radio transmitter (Tx) is responsible to send a synchronization (SYN) request to the edge device, and once it sends a SYN packet, a timer for receiving an acknowledgement (ACK) is started accordingly. The cognitive radio receiver (Rx) triggers communication once it receives the ACK packet from the edge device within the time buffer. The proposed cognitive radio (Tx/Rx) with a fast start-up further reduces communication latency. On the other hand, the edge device will function as a cluster center, monitoring the spectrum usage and communicating with IoT nodes. The fast chip-level spectrum sensor at the edge, unlike those on IoT nodes that detect low energy, will select channels whose state changes from low energy to high energy (i.e., where the connection request from the IoT node might have occurred).

In addition, powerful computation resources such as Graphic Processing Units (GPUs) can be utilized on the edge device to enable the fine-grained detection in selected channels. The waveform in selected channels are acquired by the cognitive radio receiver and will be processed by DNN classifier to generate a more detailed classification map in the frequency domain.

Fig. 3 depicts the methodology for spectrum sensing and signal classification to establish incumbent user-aware dynamic spectrum access in the identified band between the IoT node and edge device. When the communication between the IoT node to edge device is intended, the spectrum sensor on the IoT node begins to scan the sub-6 GHz range in windows of 40 MHz to detect the signal energy in each band. In this way, the

spectrum sensor continues to locate an unoccupied (or partially occupied) spectral band to be used for communication. Once a free band is identified, the IoT node sends a SYN request to the edge device. The edge device, in the meantime, will keep scanning the spectrum periodically with the fast chiplevel spectrum sensor. Once occupied (or partially occupied) channels are detected based on energy contents, the DNN classifier will perform further more accurate spectrum analysis in those channels. If there is no collision between the IoT packet and other incumbent signals, the edge device will send an ACK packet within the identified band, and hence establish a communication link with the newly registered IoT device. Otherwise, if there is congestion in the channel or if the IoT device does not receive the ACK packet back, then the connection is closed and the IoT node will choose another free channel for re-transmission after the expiration of the ACK timer. Once the communication link between the IoT node and edge device is established, the DNN classifier continues to process the signal in the band. In case the incumbent user is detected, the edge device will close the connection, causing the IoT node to rescan for the next available band. This feature classification, performed at the edge device, overcomes the blind detection limitation of the energy detection-based spectrum sensing.

A. Discussion on the packet structure

Without loss of generality, we consider the case when one IoT node communicates with an edge device. In Fig. 4, we present transmission timing details for the spectrum sensing and agile communication. The IoT node first scans the complete sub-6 GHz band for a time of t_{IoT_sense}. Once a free channel is detected, the IoT node sends a SYN packet at t_{IoT_start} to connect with the edge device, and initiates the timer with t_{IoT_ACK_timer} for handshaking. Once the edge device detects the occupied channel, it begins to acquire time domain in-phase/quadrature-phase (I/Q) samples in that channel during t_{ML_IQ_ACQ}, and afterwards performs fine-grained detection during t_{ML_classify}. It sends an ACK packet immediately if the IoT signal is detected without concurrent incumbent signal. A timer is set

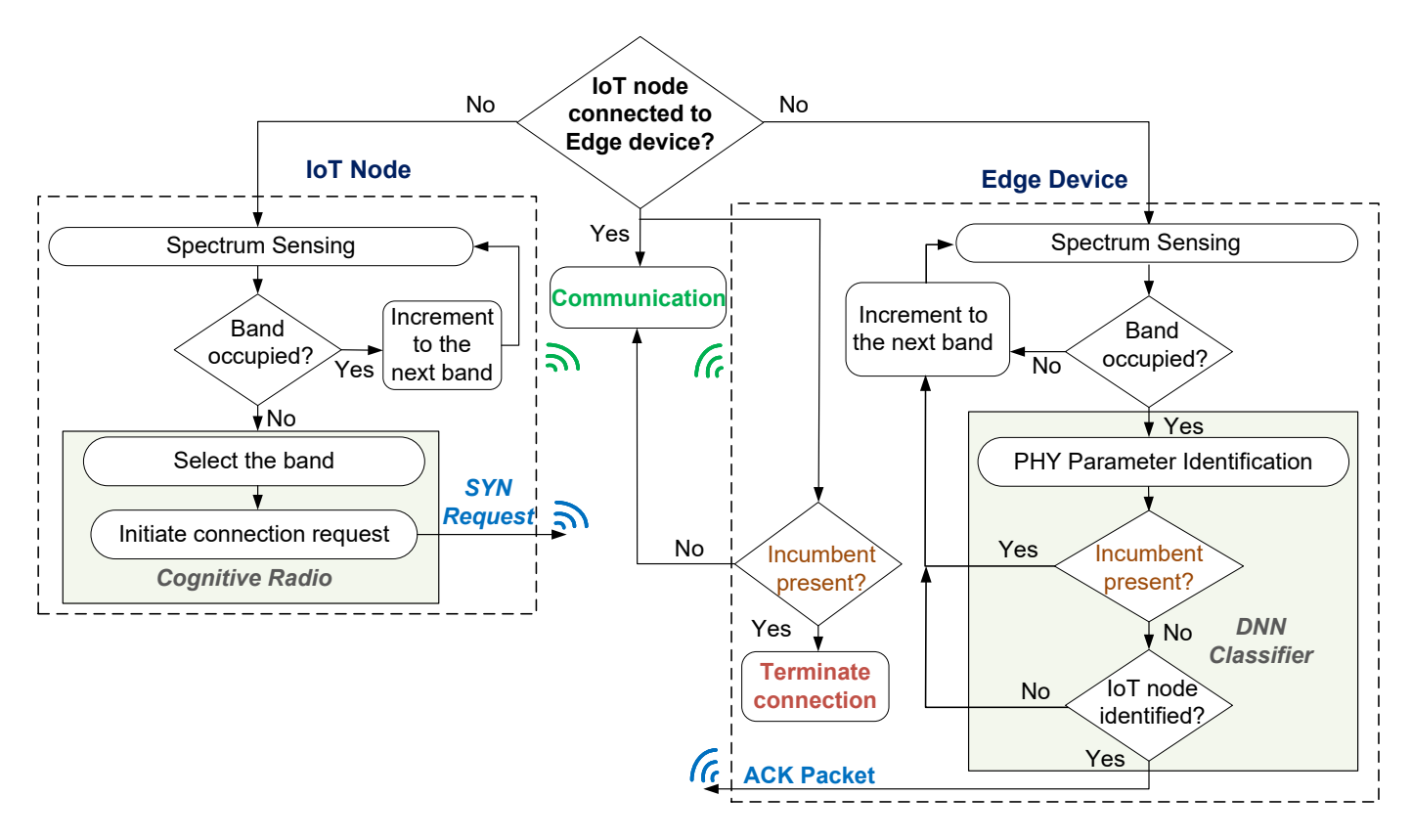


Fig. 3. Flowchart depicting the incumbent-aware spectrum sensing for dynamic spectrum access.

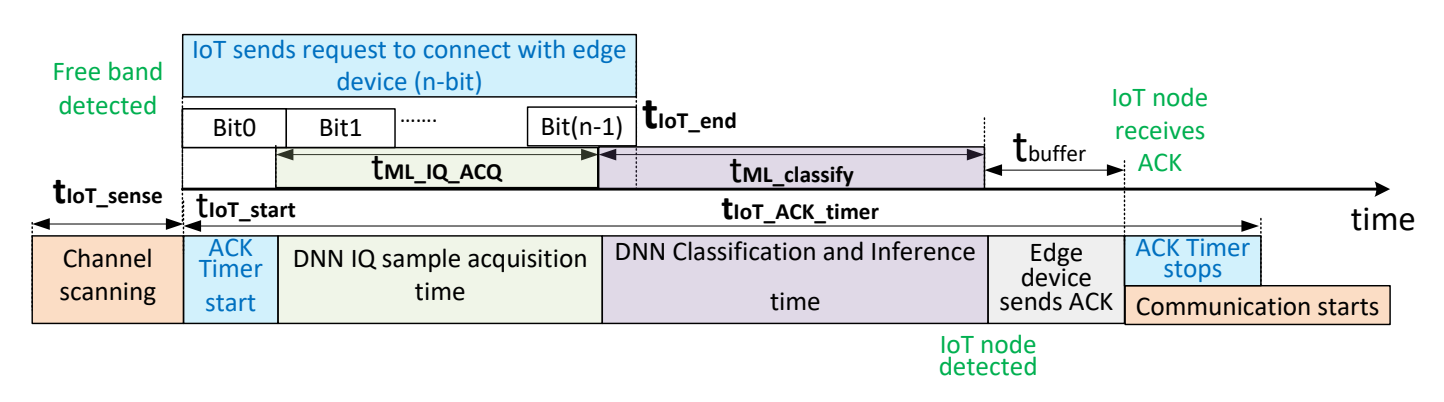


Fig. 4. Packet structure and transmission timings for dynamic spectrum access.

as $t_{IoT_ACK_timer} = t_{ML_IQ_ACQ} + t_{ML_classify} + t_{buffer}$, where t_{buffer} is a buffer time for receiving the ACK. Once the IoT node receives the ACK packet, it starts to communicate with the edge device. If the IoT node does not receive ACK packet within $t_{IoT_ACK_timer}$, it automatically begins to re-scan the sub-6 GHz band for any spectral opportunities.

III. On-Chip Spectrum Sensor

Fig. 5(a) shows the block diagram of the proposed agile energy detection-based RF spectrum sensor, in which spectrum sensing is performed using programmable active resonators with high-Q factors designed using transconductance (g_m) stages. The tunability feature offered by g_m -C filters has been proven advantageous in the design of tunable-bandwidth filters [34]–[37]. The proposed on-chip spectrum sensor will

sweep the sub-6 GHz frequency range in less than 1μ s to identify available channels for communication. Furthermore, it will use the active resonators to enable transmission and reception of RF signals. The proposed on-chip analog spectrum sensor is comprised of a tunable filter followed by energy detection in the tuned band. We use tunability for the center frequency and the resonance bandwidth of the circuit. This technique is rooted in the analog domain without high-frequency, high dynamic range analog-to-digital converters (ADC) as required by approaches that are entirely based on digital signal processing (DSP). Active resonators also play a critical role in reducing the power consumption and start-up time for transceiver designs, which are discussed in the following subsection.

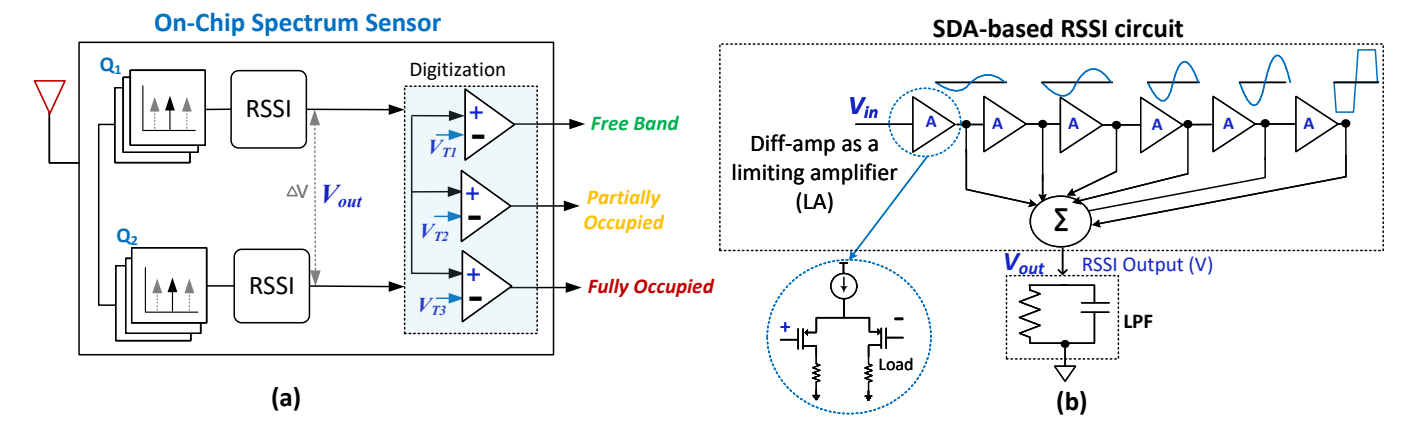


Fig. 5. (a) Proposed energy detection-based on-chip analog spectrum sensor where, V_{T1} , V_{T2} , V_{T3} represent the threshold levels of the comparators to classify the congestion levels of the sensed spectrum, and its (b) received signal strength detection using a successive detection architecture (SDA) based RSSI circuit.

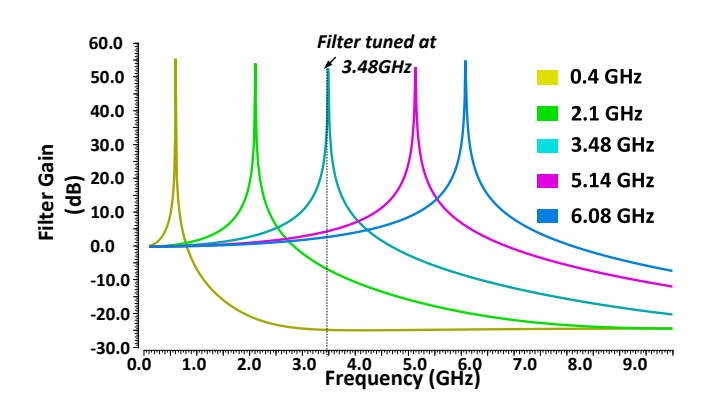


Fig. 6. On-chip tunable filter circuit SPICE simulation results.

A. On-chip Tunable Filter

Wideband sensing can be accomplished using two active resonators with same resonance frequency (ω_o) but different quality factors $(Q_1 \text{ and } Q_2)$. The proposed on-chip filter is a second-order system, and can be represented by the standard form of second-order system:

$$H(s) = \frac{\omega_o^2}{s^2 + \frac{\omega_o}{Q}s + \omega_o^2}.$$
 (1)

Tunability of ω_o and the scanning bandwidth is achieved by varying the parameters in (1). In Fig. 6, we present the SPICE simulation results of a tunable active resonator design. At resonance, the filter would amplify the incoming RF signal. In case there is RF power contents at ω_o , each active resonator will provide different gain for the incoming signal owing to their different Q factor. Consequently, a differential voltage (ΔV) will be developed at the output of the RSSI circuit as labelled in Fig. 5(a). However, absence of RF power at ω_o will result in $\Delta V \approx 0$, indicating the availability of that channel for agile communication. The proposed differential sensing technique will also help in reducing the noise level, thereby making the design more sensitive.

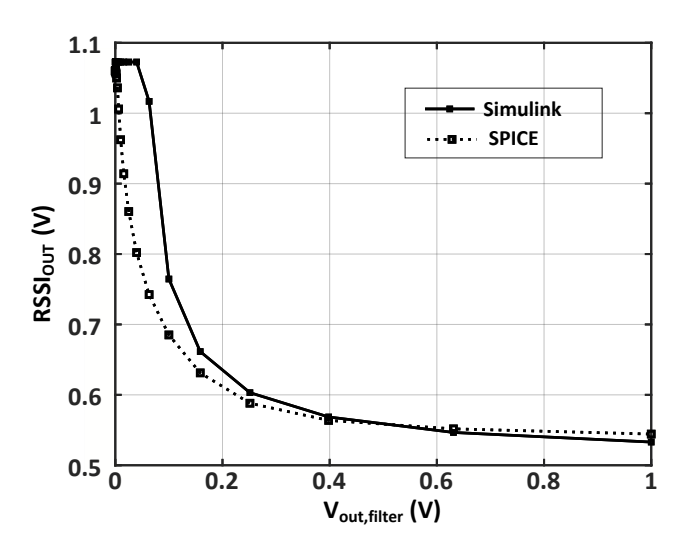


Fig. 7. Comparison of RSSI circuit and model simulation results. $V_{out,filter}$ is the input to the RSSI circuit obtained from the output of the on-chip filter, and RSSI_{OUT} is the output of the RSSI circuit.

B. Received Signal Strength Indicator

RSSIs are routinely used to control gain by obtaining the power level of the incoming signal [38]–[42]. Fig. 5(b) shows the block diagram of an successive detection architecture (SDA)-based RSSI circuit that we implemented using five differential amplifier (diff-amp) based limiting amplifiers. The incoming signal V_{in} is amplified in each stage of the cascaded amplifier with a gain A. This amplified signal moves through the chain of amplifiers. It will accordingly be limited/clipped at the saturation voltage level (V_S). The output of each stage is summed and filtered using a low-pass filter (LPF), which removes the ripple from this output to provide a DC signal V_{out} that corresponds to the power of the incoming signal. This RSSI exhibits a logarithmic characteristic, enabling signal strength detection.

$$V_{out} = \sum_{i=1}^{N} A^i \cdot V_{in}. \tag{2}$$

Equation (2) represents the output of the $i + 1^{th}$ stage as

the sum of the outputs of each stage and depending on the input amplitude, where the output of each stage may or may not be saturated. The proposed RSSI circuit will be used to perform two main functions. First, in the spectrum sensing mode of the CR-system, the RSSI will provide the power level of the received RF signal. In a receiver system, the RSSI output information will be used to control the gain of a lownoise amplifier (LNA) to prevent the saturation of the output in the receiver path through automatic gain control (AGC). In Fig. 7, we present the simulation results of the SDA-based RSSI circuit.

C. Digitization

To classify the bands, we have implemented adaptive threshold-based comparators, which classify the channel based on the energy detected in that band into fully occupied, partially occupied, and free band (or black, gray and white [43]). The RSSI circuit, which outputs a DC value corresponding to the signal energy level, enables processing of the signals in the baseband. This allows to implement a coarse classification of the detected spectral energy using ultra-low power comparators [41], [44].

Formally, in a binary classification scenario, let H_0 and H_1 denote the hypotheses of the free and occupied bands, respectively. Considering a Bayesian detection case, given an observation r, the decision is determined by

$$\frac{P(r|H_1)}{P(r|H_0)} \underset{H_1}{\overset{H_0}{\leq}} \frac{P(H_0)}{P(H_1)},\tag{3}$$

where $P(r|H_0)$ and $P(r|H_1)$ are conditional probabilities of r given by H_0 and H_1 respectively, while $P(H_0)$, $P(H_1)$ are prior probabilities of H_0 , H_1 respectively.

Equation (3) can be fully described by its sufficient statistics – the voltage value V_{out} of the RSSI circuit and a detection threshold V_t :

$$V_{out} \underset{H_1}{\overset{H_0}{\leqslant}} V_t. \tag{4}$$

We note that $P(H_0)$ and $P(H_1)$ on the IoT node side should be different from the prior probability on the edge device side. This is because the IoT node tends to transmit, resulting in a larger $P(H_0)$; while the edge device aims to detect occupation, resulting in a larger $P(H_1)$. To this end, the threshold V_t should be different at the edge device and IoT node. Let V_{t1} and V_{t2} denote the threshold at the edge and IoT node respectively, then (4) can be rewritten as

$$V_{out} \underset{H_1}{\overset{H_0}{\lessgtr}} V_{t1}, \tag{5}$$

$$V_{out} \underset{\bowtie}{\stackrel{H_0}{\lessgtr}} V_{t2}, \tag{6}$$

where (5) characterizes the decision boundary at the edge while (6) denotes the decision boundary at IoT nodes.

To unify (5) and (6), we redefine $V_{t1} \leq V_{out} \leq V_{t2}$ as "partially occupied". Let H_0 , H_1 and H_2 denote the hypotheses of free, partially occupied and fully occupied bands, such that the classification problem is determined by

$$V_{t1} \underset{H_0}{\overset{H_1 \cup H_2}{\leq}} V_{out} \underset{H_2}{\overset{H_0 \cup H_1}{\leq}} V_{t2}. \tag{7}$$

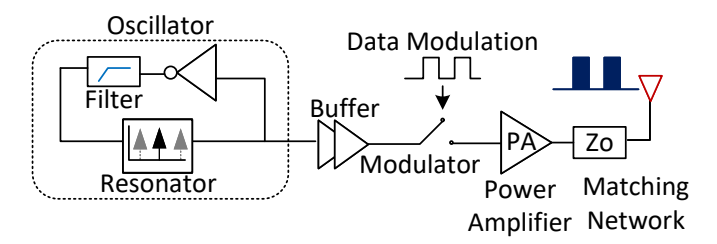


Fig. 8. Cognitive transmitter that utilizes the active resonator for carrier frequency generation, thereby significantly reducing the communication latency.

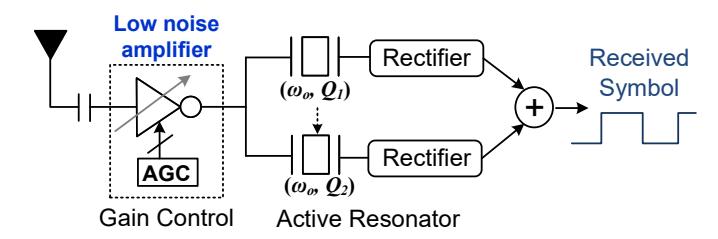


Fig. 9. Cognitive receiver consisting of an LNA with gain control followed by an active resonator and a rectifier for data acquisition.

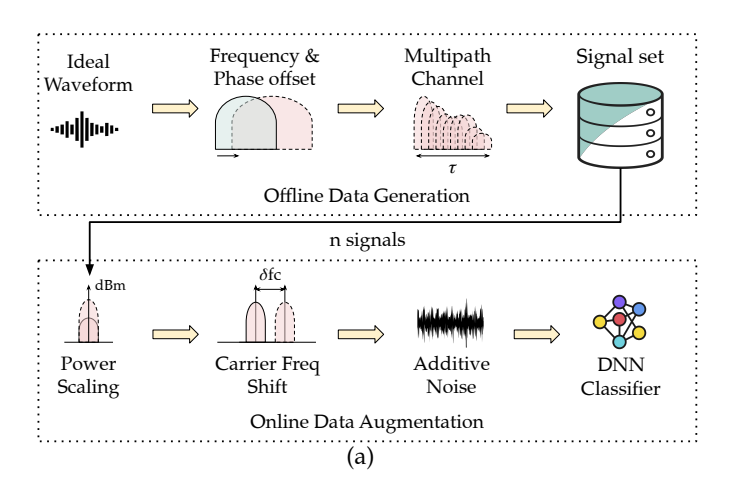
Equation (7) implies that on-chip spectrum sensors will have different Bayesian test thresholds V_{t1} and V_{t2} at the edge and IoT respectively, classifying the channel into "free", "partially occupied" and "fully occupied". The edge device will further perform fine-grained detection in "partially occupied" and "fully occupied" channels, while IoT devices tend to transmit in "free" or "partially occupied" channels.

D. Cognitive Radio Transmitter

Another critical requirement besides short spectrum sensing time is the ability of the transmitter to quickly tune parameters in order to utilize the identified spectral opportunity. The lowstartup time of the oscillator at high frequency ensures low latency in the transmission. In the proposed transmitter architecture, we utilize the active resonator for oscillator design to generate the carrier frequency corresponding to the spectral opportunity. With this design approach, we benefit from the active resonator's characteristics to enable transmission in the band. Once the channels are known, they can be utilized for communication, which requires the generation of the carrier frequency for the selected channel. We leverage the active resonator to generate such carrier frequency. In this case, the resonator is connected across a high-bandwidth inverting amplifier as shown in Fig. 8, which creates an oscillator whose resonance frequency is determined by the resonator. This signal is modulated by a modulator based on the data stream. The modulated signal is then amplified by a power amplifier (PA) and transmitted wirelessly after passing through a matching network (Z_o) .

E. Cognitive Radio Receiver

Fig. 9 displays the design of the cognitive receiver architecture. A wideband LNA circuit will be used to amplify the RF signal. A parallel AGC using an RSSI is used to prevent the receiver from saturating. The LNA output is fed to the active resonators operating differentially as discussed earlier. The



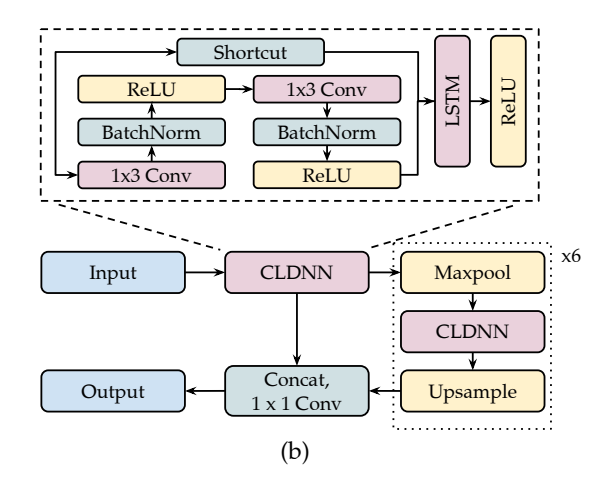


Fig. 10. (a) Data preprocessing pipeline for spectrum classification; (b) DNN architecture for spectrum classification.

output of the both resonators are fed to rectifiers to demodulate the signal. The rectifier outputs are then summed together to remove out-of-band and adjacent channel interferers. The final output represents the received symbols.

IV. DNN CLASSIFIER

This section discusses the signal model used for simulation, and it summarize the data processing as well as the DNN architecture for signal classification.

A. Signal Model

Similar to other modulation classification works [18], [45], we model the wireless imperfection as three parts:

- Multipath effects: self-interference due to the reflection, diffraction, diffusion and movement of objects, usually described by statistic models such as Rayleigh and Rician channels with different delay spread τ and Doppler shift δf_d .
- Frequency and phase offsets: frequency and time domain mismatches caused by drift of local oscillators that can be described by a random clock offset δc .
- Additive noise: hardware sensitivity that can be modeled as a stationary Gaussian random process with different power levels.

Since we process the signal after down-conversion, here we are only interested in the distortion of the low-pass (baseband) equivalent signal. Without loss of generality, we denote the transmitted signal s(t) as a baseband complex sinusoid:

$$s(t) = e^{j2\pi f_S t}. (8)$$

In (8), s(t) is a ideal waveform without any imperfection and f_s is the sampling frequency of the baseband signal. The received signal r(t) can be written as

$$r(t) = s'(t) \otimes h(t) + n(t)$$

$$= \sum \alpha(\tau)e^{-j2\pi\delta f_d \tau}s'(t-\tau) + n(t).$$
(9)

Equation (9) indicates that the received signal r(t) is modeled as the convolution of a distorted signal s'(t) with a finite impulse filter h(t) and an additive factor n(t), where h(t) is the

 $\label{table in table i} \textbf{TABLE I}$ Parameters for data generation and preprocessing

Parameters	Values
Maximum clock offset Δc (ppm)	5
Delay spread τ (μ s)	[0, 1.8, 3.4]
Maximum doppler shift Δf_d (Hz)	10
Number of signals in channel n	U(1,4)
Carrier frequency shift δf_c (MHz)	U(-20,20)
Signal to Noise Ratio (dB)	U(0, 18)

channel model and n(t) is additive noise. s'(t) is the distorted version of (8) due to the frequency and time domain mismatches between transmitter and receiver.

In (9), h(t) can be modeled as a linear filter whose impulse response describes the phase shift and attenuation of the multipath components. It is usually characterized by statistic models such as Rayleigh and Rician distribution with the delay spread τ as well as Doppler shift δf_d [46].

s'(t) can be written as

$$s'(t) = e^{j2\pi(f_s + \delta f_t + \delta f_c)t + \delta \phi_t}.$$
 (10)

In (10), δf_t and $\delta \phi_t$ are the frequency and phase shifts characterized by a random clock offset δc . As the spectrum sensor performs blind detection to the transmitted signal, the receiver has no knowledge about the carrier frequency f_c of the exact transmitted signal. δf_c is the carrier frequency mismatch between the transmitter and receiver.

B. Data Generation and Preprocessing

Due to the susceptibility of wireless signals to environmental changes and additive noise, a DL algorithm that performs well on one dataset may fail to generalize to another. Therefore, it is crucial to gather an adequate dataset from diverse environments to ensure the robustness of deep learning algorithms. However, the challenge lies in how to collect such a varied dataset, which remains an open problem [47]. This problem becomes more severe in wideband spectrum sensing scenarios because spectrum is an open resource, where unmanageable interference exists without clear labeling. As a compromise, synthetic datasets generated with realistic wireless models are

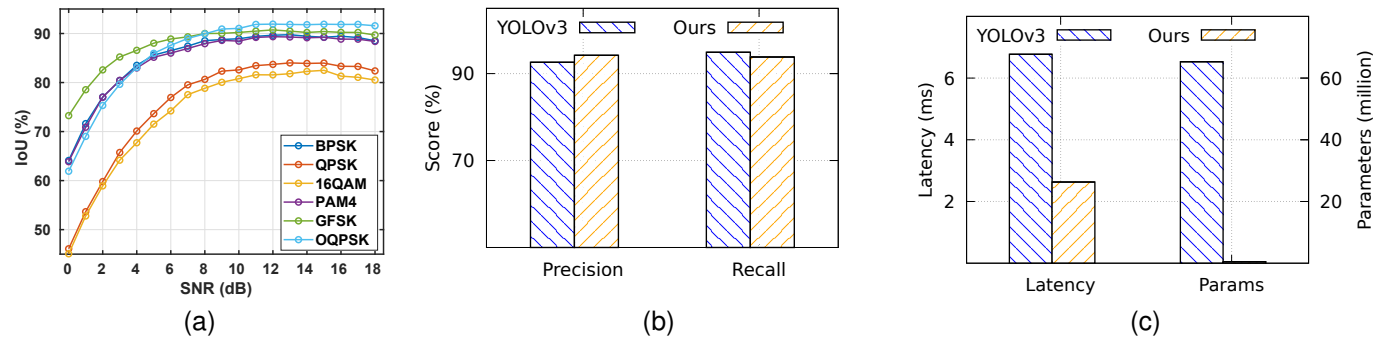


Fig. 11. (a) DNN classification performance under different SNR levels (from 0 to 18 dB); (b) precision and recall comparison between our DNN and the state of the art [27]; (c) complexity and latency comparison between our DNN and the state of the art.

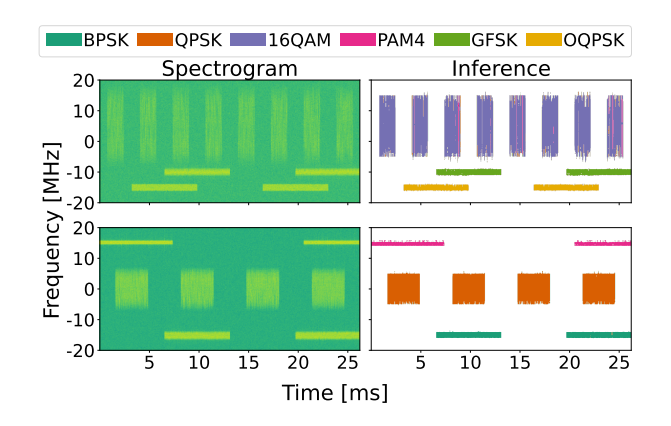


Fig. 12. Synthetic spectrograms and classification maps with different SNR and bandwidth: (Top) 16-QAM (20 MHz), GFSK (2 MHz) and OQPSK (2 MHz) with 3 dB; (Bottom) PAM4 (1 MHz), QPSK (5 MHz) and BPSK (2 MHz) with 10 dB.

commonly used to validate the efficacy of DL models in the literature [18], [23], [24], [45], [48]. To this end, we have developed a data generation pipeline capable of simulating the wideband spectrum.

To simulate a real shared spectrum, an abundant signal set containing multiple modulation and bandwidth is needed. We generated a signal set consisting of 6 different modulation types that are often used in the literature [45], [48]–[50]: *BPSK*, *QPSK*, *8PSK*, *16-QAM*, *GFSK*, *CPFSK*, *PAM4*, and *OQPSK*. For each type of modulation, 1,000 instances were generated with random bandwidth from 1 MHz to 20 MHz.

For the frequency and phase offsets, we model δc as a random variable that is uniformly distributed $U[-\Delta c, \Delta c]$, where Δc is the maximum clock offset. The carrier frequency mismatch is uniformly distributed ($\delta f_c \in U[-20,20]$ MHz). Similarly, the maximum Doppler shift Δf_d is used for modeling movement ($\delta f_d \in [-\Delta f_d, \Delta f_d]$). We selected both Rayleigh and Rician channels for a realistic simulation. Noise power is described by various SNR values from 0 to 18 dB. We do not consider signals with lower SNR because the DNN signal classifier acts after the on-chip spectrum sensor to classify signals with high RSSI outputs. Furthermore, since we are solving the signal co-existence problem in the 40 MHz band, we should also consider a random number of signals between 1 and 5 that co-exist in the spectrum. The simulation parameters

are summarized in Table I.

Fig. 10(a) depicts the proposed data generation and preprocessing pipeline to create an adequate spectrum dataset. It can be divided into two parts: offline data generation and online data augmentation. In the offline data generation phase, a set of ideal waveforms with various modulation types and bandwidths are first generated. Then, a random frequency and phase offset is introduced to each instance, followed by a Rayleigh or Rician channel fading. The generated signals are stored in a signal set for further preprocessing before feeding them to the DNN classifier. In the online data augmentation phase, a random number of signals from the signal set will be sampled and stitched together to generate a wideband spectrum. The power of each signal will be adjusted based on its SNR level. Subsequently, the carrier frequency of each signal will be shifted randomly from -20 MHz to 20 MHz. The ultimate output of the online data augmentation is a superimposition of multiple signals and random additive noise, simulating the coexisting transmissions in the 40 MHz channel. In each generated spectrum data, the number of signals, SNR, and carrier frequency are randomized. To this end, our data processing pipeline is able to have an exhaustive combination with a finite signal set.

C. DNN architecture

Inspired by semantic segmentation, we propose a new DNN architecture based on a Fully Convolutional Network (FCN) [51] to perform I/Q level classification in the frequency domain. It will take 1024 I/Q samples in the time domain, and output a classification map that represents 1024 channels in the frequency domain. Unlike the original FCN, we utilize a Convolutional-LSTM-DNN (CLDNN) structure that has shown its efficacy for signal processing in [52] for feature extraction. Fig. 10(b) depicts the detail of our proposed model architecture. the CLDNN has 2 convolutional layers $(1 \times 3 \text{ Conv})$ and a Long Short-Term Memory (LSTM). After each convolutional layer, there is a batch normalization and a rectified linear unit (ReLU) activation, whereas the LSTM is only followed by ReLU activation. A shortcut is used as the residual connection [53] between the input and LSTM. The complete FCN comprises 7 CLDNN blocks designed to produce feature maps with varying levels of granularity. These levels are adjusted by incorporating maxpooling layers (maxpool) between each

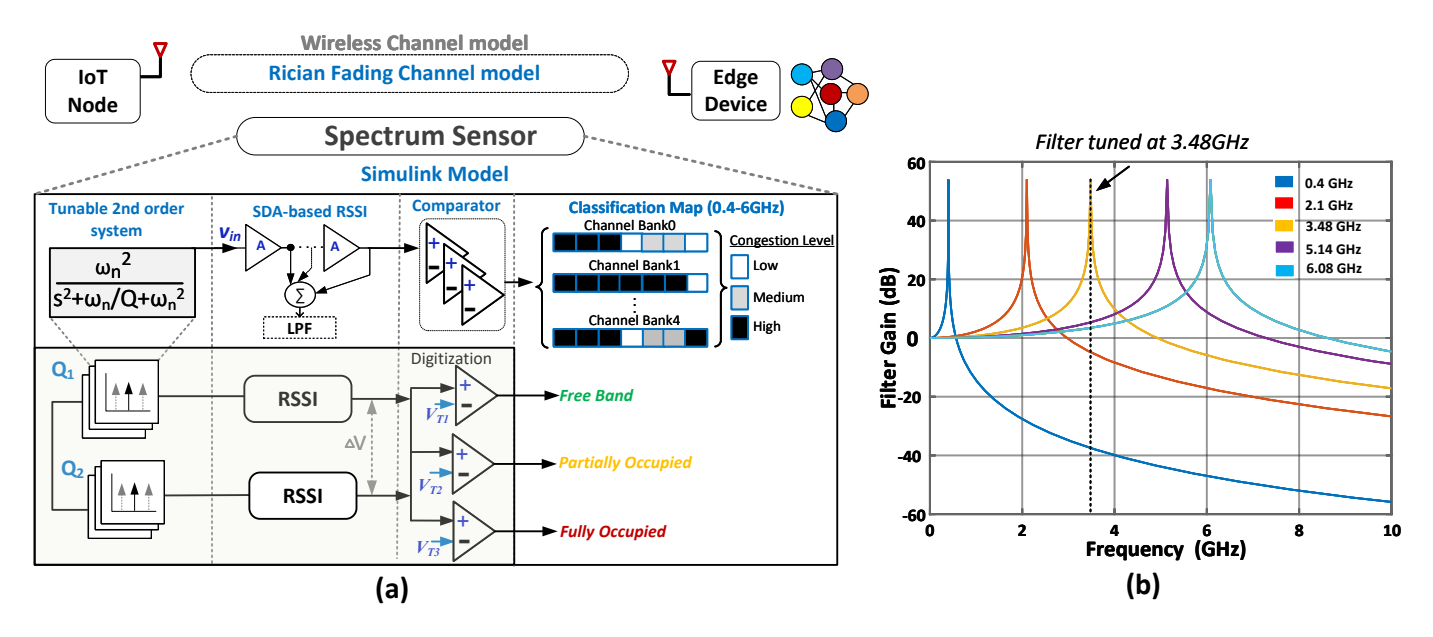


Fig. 13. (a) System architecture of the proposed analog spectrum sensor and the corresponding system modeling. (b) Results from simulation of the Simulink-based tunable filter model.

CLDNN block. To decode these feature maps, a series of upsampling layers (upsample) of different scales are initially applied to resize the feature maps to their original dimensions. Subsequently, a concatenation layer (concat) followed by a pointwise convolution $(1 \times 1 \text{ Conv})$ is employed to blend the diverse features and generate the classification map.

Different from other signal classification works that can only classify one signal at its center frequency [48]–[50], our approach can generate a classification map in a wideband spectrum that can jointly classify multiple signals at different center frequencies. Compared to other signal classification based on vision-driven object detection [26], [27], we directly process the 1-dimensional waveform data and do not transform to image, resulting in less computation complexity and latency.

D. DNN Performance

We report the instance level classification performance of our DNN in Fig. 11(a), where the Intersection-over-Union (IoU) metric from computer vision tasks was adopted to evaluate the instance level performance. For each instance (i.e., 1024 I/Q samples in the time domain), we compute the miss rate (P_m) , false alarm rate (P_{fa}) and detection rate (P_d) over the classification map (i.e., classification of 1024 frequency channels). The IoU is computed as

$$IoU = \frac{P_d}{P_m + P_d + P_{fa}}. (11)$$

Equation (11) denotes the IoU metric; where P_d , P_m and P_{fa} are detection rate, miss rate and false alarm rate, respectively.

When SNR increases from 0 to 6 dB, the average IoU increases from 59.05% to 83.36%. The average IoU is up to 86.84% under 18 dB SNR, with only 3.48% improvement. The experimental results show the stable performance of our approach for various SNRs. This SNR range is guaranteed by

the on-chip spectrum sensor deployed at the edge since we only classify signals in the occupied channels.

Note that the IoU is a more comprehensive performance metric than other metrics such as precision and recall scores that are computed as

$$Precision = \frac{P_d}{P_d + P_{fa}},\tag{12}$$

$$Recall = \frac{P_d}{P_m + P_d}. (13)$$

Equation (12) and (13) denote the precision and recall scores, respectively. Compared to (12) and (13), (11) always has a lower score as P_m and P_{fa} are non-negative. In other state of the art [27], the IoU is only treated as an optimization metric while precision and recall are used for evaluation. This is because [27] directly applies to computer vision based object detectors, which relies on a set of predefined anchors. Such predefined anchors will introduce bias to the objects' locations and shapes, showing difficulty to achieve very precise IoU score [28], [54]. On the other hand, our approach is based on semantic segmentation [51] that can provide better information about the objects' boundaries.

We compare the classification performance with the state-of-the-art technique that can classify multiple signals in the spectrum using a YOLOv3 object detector [27]. To ensure a fair comparison, we present precision and recall scores similar to [27]. In a scenario with moderate SNR (10 dB), our segmentation approach achieves 94.2% precision and 93.8% recall rates, respectively. These rates are approximately 10% higher than the IoU metric, supporting that the IoU is more comprehensive for performance evaluation. On the other hand, the object detection-based approach achieves a precision rate of 92.6% and a recall rate of 94.9%. As depicted in Fig. 11(b), it has less than 2% difference in classification performance between our method and the current state of the art.

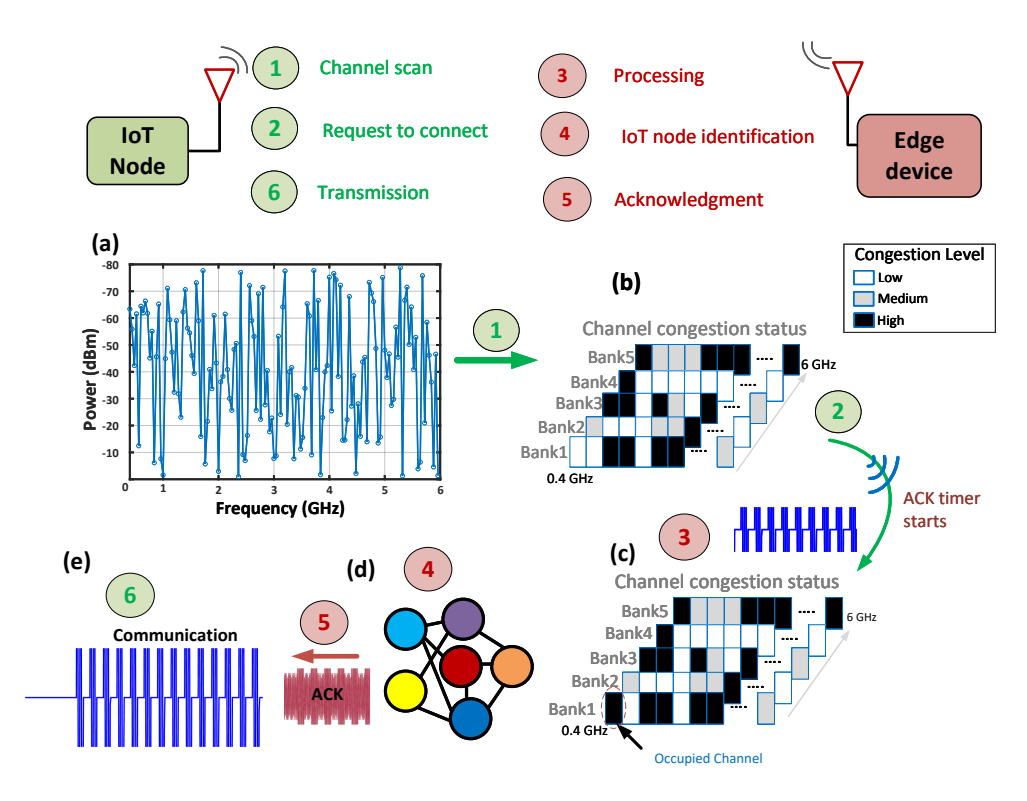


Fig. 14. Simulation of spectrum sensing and communication between an IoT node and edge device.

We also compare the computation complexity and latency of our model with YOLOv3 [27]. Fig. 11(c) shows the inference latency and number of parameters of YOLOv3 and our approach. The latency is tested on a Linux machine with a 12th Generation Intel(R) Core(TM) i7-12700K and a GPU RTX-A4000 with a 7.5 computation capability. The YOLOv3 latency is evaluated following the same setup as in [27]. The latency of our approach is 2.63 ms while the YOLOv3 has a latency of 6.77 ms. Compared to the state of the art, our DNN reduces the latency by 61.15%. In addition, the parameter number of YOLOv3 is 65.3 million while ours is only 0.46 million. Note that the computation resources and latency can be further reduced by implementing the DNN on a Field-Programmable Gate Arrays (FPGAs) or as an Application-Specific Integrated Circuit (ASIC) [55].

Based on the comparisons discussed above, our approach demonstrates similar classification performance while exhibiting significantly reduced latency compared to the current state of the art. This is because the other works are currently derived from computer vision tasks, which were originally tailored for extracting high-level information from 2-dimensional pixels, resulting in excessive computational overhead for wireless tasks. On the other hand, our approach operates directly on the 1-dimensional waveform-level features of signals, drastically reducing complexity while maintaining equivalent accuracy levels.

Fig. 12 shows two different scenarios of spectrograms and the related DNN outputs. The synthetic spectrum is generated by our data generation pipeline depicted in Fig. 10(a). The classification map is a horizontal stack of multiple DNN outputs in the time domain. The DNN can classify multiple signals with

different bandwidths, center frequencies and different SNR in the spectrum. We note that the classification accuracy can be further enhanced by aggregating multiple DNN outputs in the time domain with low SNR scenarios. With the powerful parallel computing provided by the GPU on the edge device, the performance can be easily enhanced without increasing the latency.

V. SYSTEM MODELING

The proposed on-chip spectrum sensor validation is heavy on computational resources when done using circuit level simulations. To overcome this, we validate the proposed analog spectrum sensing technique using a system model implemented in MATLAB-Simulink. Circuit-level non-idealities have been considered in the implementation of the system model based on the techniques in [56], [57]. Fig. 13(a) visualizes the Simulink modeling of different components of the spectrum sensor. The modeling details for different blocks are discussed below.

A. Channel Model

To model the spatio-temporal non-idealities of the channel, we have used a Rician channel model as described in Section IV-A. We have evaluated our model with unmodulated continuous wave On-Off Keying (OOK) and other modulation techniques listed in Section IV-B.

B. Tunable On-chip Filter

The proposed on-chip filter is modeled using a second-order system as described by Eqn. 1. To achieve tunability we vary ω_o and the Q-factor in the sub-6 GHz range. Furthermore, we

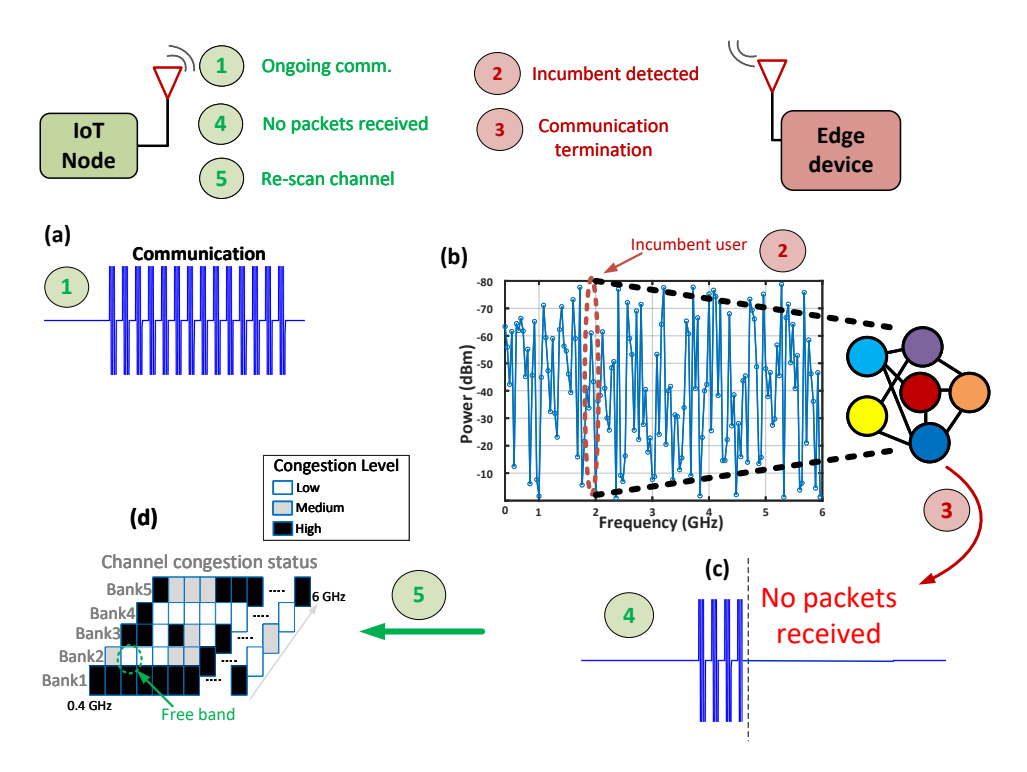


Fig. 15. Simulation of spectrum sensing and communication between an IoT node and edge device when the incumbent user intends to use the channel.

use the active resonators in a differential topology to reduce the effects of the out-of-band blockers (Section III-A). Fig. 13(b) displays the Simulink model-based simulation results, which are in close agreement with the circuit level (g_m -C filter-based) simulation results (Fig. 6).

C. RSSI Circuit

The RSSI model was implemented in Simulink, which is based on the SDA RSSI topology discussed in Section III-B. To accurately model the RSSI circuit, we have designed it using five stages of cascaded differential amplifiers followed by a summing circuit. The final output is generated after filtering with a low-pass filter. Fig. 7 compares the transistor-level RSSI circuit simulation results with the results from the Simulink model, which are monitored at the low-pass filter ($V_{out,filter}$) while processing the output of a 6 GHz active resonator with inputs varying from 0.1 mV to 1 V. The Simulink model implementation shows a dynamic range similar to the simulated transistor-level circuit design.

D. Digitization and classification map

For a coarse classification of the detected energy level, we have implemented the digitization block using three comparators to classify the channel into fully occupied, partially occupied and free bands. To make the decision threshold level adjustable, we have included a tunable voltage range in the model.

E. Cognitive Transmitter and Receiver

We have modeled the cognitive transmitter and receiver similar to its circuit implementation (Fig. 8 and Fig. 9). The spectrum sensors on the IoT node and edge device have the same architecture. However, while the spectrum sensor on the IoT node scans for a free channel, the spectrum sensor on the edge device looks for an occupied channel for further processing.

F. Simulation Results

1) Spectrum sensing and communication: Fig. 14 includes an example simulation result with free channel identification and communication on that free channel. The IoT node spectrum sensor begins to scan the channel, performs energy detection in each band, and obtains a congestion map. Using this congestion map, the free channel is identified, and the IoT node's cognitive transmitter sends a connection request to the edge device for connection in this free band. Meanwhile, the spectrum sensor on the edge device is scanning the sub-6 GHz band for congested channels.

These congested channels are then processed for IoT node identification as discussed in Fig. 3. Fig. 14 shows the change of the energy in the previously free channel that is now occupied from the signal from the IoT node. The coarse classification of channels obtained from the spectrum sensor are then processed by the DNN classifier. The DNN will further perform fine-grained signal classification only in the channel whose state changed from free to occupied. It will output a classification map of the spectrum as demonstrated in Fig. 12. Once the IoT node is identified, the edge device sends the ACK packet to the IoT node. This handshake between the IoT node and edge device establishes the intended communication.

2) Detection of an incumbent user: Fig. 15 depicts a scenario wherein the incumbent user of the channel intends to use the channel in which the IoT node is opportunistically commu-

nicating with the edge device. In this case, the DNN classifier identifies the incumbent user and terminates the connection with the IoT node. Once the edge device stops transmitting the packets, the timer on the IoT node detects the termination of the connection from the edge device, and the IoT node begins to scan the channel for the next available band as discussed in Fig. 3. This response overcomes the blind detection limitation of conventional energy detection-based spectrum sensing, which in our agile platform involves offloading to the edge device to improve the energy efficiency of the low-power IoT devices.

VI. CONCLUSIONS

This paper described an agile communication platform for spectrum sensing and communication for congested networks of IoT devices. To achieve fast spectrum sensing, we have introduced an energy detection-based approach that leverages an on-chip analog spectrum sensor to scan the sub-6 GHz band in less than 1μ s. A novel DL-based algorithm achieves a mean IoU up to 86.8%, which was employed to classify multiple signals jointly in the shared spectrum for enhanced spectrum agility. The sensing and communication methodology was assessed with Simulink-based system modeling and simulations. The agile platform overcomes past limitations associated with energy detection-based spectrum sensing (i.e., narrowband sensing and blind detection), while allowing to maintain low-power IoT nodes through offloading of computations to the edge device.

Our DL approach reduces both computation complexity and latency compared to existing works, but it relies on powerful computational resources such as GPUs for efficient parallel processing to achieve low latency. In future endeavors, a potential direction is to implement the proposed DL model on FPGAs or as an ASIC to further diminish computational demands and latency. Furthermore, the DL algorithm is trained on synthetic data and the proposed framework was tested with simulations. Future work may involve deploying a hardware implementation to test devices with real data collected in the field.

REFERENCES

- [1] Z. Yang, B. Liang, and W. Ji, "An intelligent end–edge–cloud architecture for visual IoT-assisted healthcare systems," *IEEE Internet Things J.*, vol. 8, no. 23, pp. 16779–16786, Dec. 2021.
- [2] S. Misra, S. Pal, N. Ahmed, and A. Mukherjee, "SDN-controlled resource-tailored analytics for healthcare IoT system," *IEEE Syst J.*, vol. 17, no. 2, pp. 1777–1784, June 2023.
- [3] W. Li, T. Logenthiran, V.-T. Phan, and W. L. Woo, "A novel smart energy theft system (SETS) for IoT-based smart home," *IEEE Internet Things J.*, vol. 6, no. 3, pp. 5531–5539, June 2019.
- [4] Y. Dong and Y.-D. Yao, "Secure mmwave-radar-based speaker verification for IoT smart home," *IEEE Internet Things J.*, vol. 8, no. 5, pp. 3500– 3511, Mar. 2021.
- [5] N. Ahmed, D. De, and I. Hussain, "Internet of Things (IoT) for smart precision agriculture and farming in rural areas," *IEEE Internet Things J.*, vol. 5, no. 6, pp. 4890–4899, Dec. 2018.
- [6] K. A. Jani and N. K. Chaubey, "A novel model for optimization of resource utilization in smart agriculture system using IoT (SMAIoT)," *IEEE Internet Things J.*, vol. 9, no. 13, pp. 11275–11282, July 2022.
- [7] Ericsson, "Ericsson Mobility Report," Ericsson, Tech. Rep., Nov. 2023.[Online]. Available: https://www.ericsson.com/en/reports-and-papers/mobility-report/reports
- [8] M. McHenry, "NSF spectrum occupancy measurements," NSF, Tech. Rep., Aug. 2005.

- [9] T. Yucek and H. Arslan, "A survey of spectrum sensing algorithms for cognitive radio applications," *IEEE Commun. Surv. Tut.*, vol. 11, no. 1, pp. 116–130, 2009.
- [10] D. Cabric, S. Mishra, and R. Brodersen, "Implementation issues in spectrum sensing for cognitive radios," in *Proc. Conf. Rec. 38th Asilomar Conf. Signals, Syst. Comput.*, Pacific Grove, CA, USA, Nov. 2004.
- [11] N.-S. Kim and J. M. Rabaey, "A high data-rate energy-efficient triplechannel UWB-based cognitive radio," *IEEE J. Solid-State Circuits*, vol. 51, no. 4, pp. 809–820, Apr. 2016.
- [12] A. Ghasemi and E. S. Sousa, "Spectrum sensing in cognitive radio networks: requirements, challenges and design trade-offs," *IEEE Commun. Mag.*, vol. 46, no. 4, pp. 32–39, Apr. 2008.
- [13] J. Park, T. Song, J. Hur, S. M. Lee, J. Choi, K. Kim, K. Lim, C.-H. Lee, H. Kim, and J. Laskar, "A fully integrated UHF-band CMOS receiver with multi-resolution spectrum sensing (MRSS) functionality for IEEE 802.22 cognitive radio applications," *IEEE J. Solid-State Circuits*, vol. 44, no. 1, pp. 258–268, Jan. 2009.
- [14] K. Banović and T. C. Carusone, "A sub-mw spectrum sensing architecture for portable IEEE 802.22 cognitive radio applications," in *Proc. IEEE Int. Symp. Circuits Syst. (ISCAS)*, Baltimore, MD, USA, May 2017.
- [15] D. Cabric, A. Tkachenko, and R. W. Brodersen, "Experimental study of spectrum sensing based on energy detection and network cooperation," in *Proc. 1st. Int. Workshop Technol. Policy for Accessing Spectrum*, Boston, MA, USA, Aug. 2006.
- [16] H. Urkowitz, "Energy detection of unknown deterministic signals," *Proc. IEEE*, vol. 55, no. 4, pp. 523–531, Apr. 1967.
- [17] H. Sun, A. Nallanathan, C.-X. Wang, and Y. Chen, "Wideband spectrum sensing for cognitive radio networks: A survey," *IEEE Wirel. Commun.*, vol. 20, no. 2, pp. 74–81, Apr. 2013.
- [18] T. J. O'Shea, T. Roy, and T. C. Clancy, "Over-the-air deep learning based radio signal classification," *IEEE J. Sel. Top. Signal Process*, vol. 12, no. 1, pp. 168–179, Feb. 2018.
- [19] K. Tekbıyık, Ö. Akbunar, A. R. Ekti, A. Görçin, G. K. Kurt, and K. A. Qaraqe, "Spectrum sensing and signal identification with deep learning based on spectral correlation function," *IEEE Trans. Veh. Technol.*, vol. 70, no. 10, pp. 10514–10527, Oct. 2021.
- [20] F. Restuccia and T. Melodia, "PolymoRF: Polymorphic wireless receivers through physical-layer deep learning," in Proc. 21st. Int. Symp. Theory, Algorithmic Found., Protocol Design Mobile Netw. Mobile Comput., France, New York, NY, USA, Oct. 2020.
- [21] S. Chang, S. Huang, R. Zhang, Z. Feng, and L. Liu, "Multitask-learning-based deep neural network for automatic modulation classification," *IEEE Internet Things J.*, vol. 9, no. 3, pp. 2192–2206, Feb. 2022.
- [22] P. Ghasemzadeh, M. Hempel, and H. Sharif, "GS-QRNN: A high-efficiency automatic modulation classifier for cognitive radio IoT," *IEEE Internet Things J.*, vol. 9, no. 12, pp. 9467–9477, June 2022.
- [23] C. Hou, G. Liu, Q. Tian, Z. Zhou, L. Hua, and Y. Lin, "Multisignal modulation classification using sliding window detection and complex convolutional network in frequency domain," *IEEE Internet Things J.*, vol. 9, no. 19, pp. 19 438–19 449, Oct. 2022.
- [24] L. Zhang, S. Lambotharan, G. Zheng, G. Liao, B. AsSadhan, and F. Roli, "Attention-based adversarial robust distillation in radio signal classifications for low-power IoT devices," *IEEE Internet Things J.*, vol. 10, no. 3, pp. 2646–2657, Feb. 2023.
- [25] F. Restuccia, S. D'Oro, A. Al-Shawabka, B. C. Rendon, S. Ioannidis, and T. Melodia, "DeepFIR: Channel-robust physical-layer deep learning through adaptive waveform filtering," *IEEE Trans. Wirel. Commun.*, vol. 20, no. 12, pp. 8054–8066, Dec. 2021.
- [26] S. Kayraklik, Y. Alagöz, and A. F. Coşkun, "Application of object detection approaches on the wideband sensing problem," in *Proc. IEEE Int. Black Sea Conf. Commun. Netw. (BlackSeaCom)*, Sofia, Bulgaria, June 2022.
- [27] H. N. Nguyen, M. Vomvas, T. D. Vo-Huu, and G. Noubir, "WRIST: Wideband, real-time, spectro-temporal RF identification system using deep learning," *IEEE Trans. Mob. Comput*, pp. 1–18, Early Access.
- [28] J. Redmon and A. Farhadi, "YOLOv3: An incremental improvement," arXiv preprint arXiv:1804.02767, 2018.
- [29] L. Baldesi, F. Restuccia, and T. Melodia, "ChARM: NextG spectrum sharing through data-driven real-time O-RAN dynamic control," in *Proc.* IEEE INFOCOM Conf. Comput. Commun., London, UK, May 2022.
- [30] Q. Meng, P. Lu, and S. Zhu, "A smartphone-enabled IoT system for vibration and noise monitoring of rail transit," *IEEE Internet Things J.*, vol. 10, no. 10, pp. 8097–8917, 2023.
- [31] Z. Sharif, L. T. Jung, I. Razzak, and M. Alazab, "Adaptive and priority-based resource allocation for efficient resources utilization in mobile-edge computing," *IEEE Internet Things J.*, vol. 10, no. 4, pp. 3079–3093, 2023.

- [32] J. Dou, G. Xie, Z. Tian, L. Cui, and S. Yu, "Modeling and analyzing the spatial-temporal propagation of malware in mobile wearable IoT networks," *IEEE Internet Things J.*, vol. 11, no. 2, pp. 2438–2452, 2024.
- [33] G. Manogaran, M. Alazab, H. Song, and N. Kumar, "CDP-UA: cognitive data processing method wearable sensor data uncertainty analysis in the internet of things assisted smart medical healthcare systems," *IEEE J. Biomed. Health Informat.*, vol. 25, no. 10, pp. 3691–3699, 2021.
- [34] S. Hori, T. Maeda, N. Matsuno, and H. Hida, "Low-power widely tunable Gm-C filter with an adaptive DC-blocking, triode-biased MOSFET transconductor," in *Proc. IEEE European Solid State Circuits Conf.* (ESSCIRC), Leuven, Belgium, Sept. 2004.
- [35] X. Wang, C. C. Boon, K. Yang, and L. Kong, "A 20–80 MHZ continuously tunable Gm-C low-pass filter for ultra-low power WBAN receiver front-end," *IEEE Access*, vol. 9, pp. 154 136–154 142, Nov. 2021.
- [36] M. A. A. Ibrahim and M. Onabajo, "Linear input range extension for low-voltage operational transconductance amplifiers in Gm-C filters," in Proc. IEEE Int. Symp. Circuits Syst. (ISCAS), Baltimore, MD, USA, May 2017.
- [37] N. Pekcokguler, D. Morche, A. Burg, and C. Dehollain, "An ultra-low-power widely-tunable complex band-pass filter for RF spectrum sensing," *IEEE Trans. Circuits Syst. I, Reg. Papers*, vol. 70, no. 10, pp. 3879–3887, Oct. 2023.
- [38] P.-H. P. Wang, C. Zhang, H. Yang, M. Dunna, D. Bharadia, and P. P. Mercier, "A Low-Power Backscatter Modulation System Communicating Across Tens of Meters With Standards-Compliant Wi-Fi Transceivers," *IEEE J. Solid-State Circuits*, vol. 55, no. 11, pp. 2959–2969, Nov. 2020.
- [39] P. S. Yedavalli, T. Riihonen, X. Wang, and J. M. Rabaey, "Far-field RF wireless power transfer with blind adaptive beamforming for internet of things devices," *IEEE Access*, vol. 5, pp. 1743–1752, Feb. 2017.
- [40] A. Buffi, A. Michel, P. Nepa, and B. Tellini, "RSSI measurements for RFID tag classification in smart storage systems," *IEEE Trans. Instrum. Meas.*, vol. 67, no. 4, pp. 894–904, Apr. 2018.
- [41] A. Mittal, N. Mirchandani, G. Michetti, L. Colombo, T. Haque, M. Rinaldi, and A. Shrivastava, "A ±0.5 dB, 6 nW RSSI circuit with RF power-to-digital conversion technique for ultra-low power IoT radio applications," *IEEE Trans. Circuits Syst. I, Reg. Papers*, vol. 69, no. 9, pp. 3526–3539, Sept. 2022.
- [42] Y. Zhang, N. Mirchandani, M. Onabajo, and A. Shrivastava, "RSSI amplifier design for a feature extraction technique to detect seizures with analog computing," in *Proc. IEEE Int. Symp. Circuits Syst. (ISCAS)*, Seville, Spain, Oct. 2020.
- [43] Z. Tian and G. B. Giannakis, "Compressed sensing for wideband cognitive radios," in *Proc. IEEE Int. Conf. Acoust., Speech Signal Process.* (ICASSP), Honolulu, HI, USA, Apr. 2007.
- [44] O. Aiello, P. Crovetti, P. Toledo, and M. Alioto, "Rail-to-rail dynamic voltage comparator scalable down to pW-range power and 0.15-V supply," *IEEE Trans. Circuits Syst. II, Exp. Briefs*, vol. 68, no. 7, pp. 2675– 2679, July 2021.
- [45] E. Perenda, S. Rajendran, G. Bovet, S. Pollin, and M. Zheleva, "Learning the unknown: Improving modulation classification performance in unseen scenarios," in *Proc. IEEE INFOCOM Conf. Comput. Commun.*, Vancouver, BC, Canada, May 2021.
- [46] A. Goldsmith, Wireless Communications. Cambridge Univ. Press, 2005.
- [47] A. Al-Shawabka, F. Restuccia, S. D'Oro, T. Jian, B. C. Rendon, N. Soltani, J. Dy, S. Ioannidis, K. Chowdhury, and T. Melodia, "Exposing the fingerprint: Dissecting the impact of the wireless channel on radio fingerprinting," in *Proc. IEEE INFOCOM Conf. Comput. Commun.*, Toronto, Canada, July, 2020.
- [48] T. Huynh-The, T.-V. Nguyen, Q.-V. Pham, D. B. da Costa, G.-H. Kwon, and D.-S. Kim, "Efficient convolutional networks for robust automatic modulation classification in OFDM-based wireless systems," *IEEE Syst J.*, vol. 17, no. 1, pp. 964–975, Mar. 2023.
- [49] S. Huang, C. Lin, W. Xu, Y. Gao, Z. Feng, and F. Zhu, "Identification of active attacks in internet of things: Joint model- and data-driven automatic modulation classification approach," *IEEE Internet Things J.*, vol. 8, no. 3, pp. 2051–2065, Feb. 2021.
- [50] S. Huang, R. Dai, J. Huang, Y. Yao, Y. Gao, F. Ning, and Z. Feng, "Automatic modulation classification using gated recurrent residual network," *IEEE Internet Things J.*, vol. 7, no. 8, pp. 7795–7807, Aug. 2020.
- [51] J. Long, E. Shelhamer, and T. Darrell, "Fully convolutional networks for semantic segmentation," in *Proc. IEEE Conf. Comput. Vis. Pattern Recognit. (CVPR)*, Boston, MA, USA, June 2015.
- [52] N. E. West and T. O'shea, "Deep architectures for modulation recognition," in *Proc. IEEE Int. Symp. Dyn. Spectr. Access Netw. (DySPAN)*, Baltimore, MD, USA, Mar. 2017.
- [53] K. He, X. Zhang, S. Ren, and J. Sun, "Deep residual learning for image recognition," in *Proc. IEEE Comput. Soc. Conf. Comput. Vis. Pattern Recognit. (CVPR)*, Las Vegas, NV, USA, June 2016.

- [54] X. Zhang, F. Wan, C. Liu, R. Ji, and Q. Ye, "FreeAnchor: Learning to match anchors for visual object detection," in *Proc. Int. Conf. Neural Inf. Process. Syst.*, vol. 32, Vancouver, BC, Canada, Dec. 2019.
- [55] F. Restuccia and T. Melodia, "Big data goes small: Real-time spectrum-driven embedded wireless networking through deep learning in the RF loop," in *Proc. IEEE INFOCOM Conf. Comput. Commun.*, Paris, France, July, 2019.
- [56] N. Mirchandani, Y. Zhang, S. Abdelfattah, M. Onabajo, and A. Shrivastava, "Modeling and simulation of circuit-level nonidealities for an analog computing design approach with application to EEG feature extraction," *IEEE Trans. Comput.-Aided Des. Integr. Circuits Syst.*, vol. 42, no. 1, pp. 229–242, Jan. 2023.
- [57] I. Martos-Repath, A. Mittal, M. Zaeimbashi, D. Das, N. X. Sun, A. Shrivastava, and M. Onabajo, "Modeling of magnetoelectric antennas for circuit simulations in magnetic sensing applications," in *Proc. IEEE Int. Midwest Symp. Circuits Syst. (MWSCAS)*, Springfield, MA, USA, Aug. 2020.



Ankit Mittal received his B. Tech. degree in Electronics and Communication engineering from Dayalbagh Educational Institute, India in 2014 where he was also the recipient of Director's medal (Valedictorian Honor). Currently he is a Ph.D. candidate in the Energy Efficient Circuits and Systems Group, Electrical Engineering at Northeastern University, USA. Prior to joining Ph.D. program, he was a senior design engineer in NXP Semiconductors, India with a rich experience in SoC design and 5 memory testchip tapeout to his credit. His research interests include

power management integrated circuit design, ultra-low power biomedical circuits, ultra-low power RF radio design.



Milin Zhang (Graduate Student Member, IEEE) is a Ph.D candidate in computer engineering in the Department of Electrical and Computer Engineering and a member of the Institute for the Wireless Internet of Things at Northeastern University. He received his M.S. in electrical engineering from Syracuse University, USA, in 2021. He received B.S. from the University of Electronic Science and Technology of China in 2018. His area of study is the integration of deep learning with emerging wireless technologies.



Thomas Gourousis (Graduate Student Member, IEEE) received the diploma degree in electrical and computer engineering from the University of Patras, Greece in 2020. He is currently pursuing the Ph.D. degree in electrical engineering with Northeastern University, Boston, MA, USA. His current research interests include analog/mixed-signal integrated circuit (IC) design, on-chip hardware Trojan detection and circuits for performance monitoring.



Ziyue Zhang is a Ph.D. candidate at Northeastern University. He is majoring in Mathematics and has several publications related to hardware security and machine learning.



Yunsi Fei (M'04-SM'19)) received her B.S. and M.S. degrees in electronic engineering from Tsinghua University, Beijing, China, in 1997 and 1999, respectively, and the Ph.D. degree in electrical engineering from Princeton University, Princeton, NJ, USA, in 2004. She is currently a Professor in the Department of Electrical and Computer Engineering, Northeastern University, Boston, MA, USA. Her recent research interests include hardware-oriented security and trust, side-channel attacks analysis and countermeasures, management and optimization of cyber-

physical systems and underwater sensor networks, energy-efficient embedded system design, and computer architecture. Dr. Fei was a recipient of the NSF CAREER Award. She served as the general co-chair for a flagship conference – Cryptographic Hardware and Embedded Systems (CHES) 2019, and has been on TPCs of many premier conferences on hardware and system security, EDA, and computer architecture. Her research group has won best paper awards in several conferences including International Symposium on Modeling, Analysis, and Simulation of Computer and Telecommunication Systems (MASCOTS) 2015, International Conference on Computer Design (ICCD) 2017, and AsiaCCS 2023



Marvin Onabajo (Senior Member, IEEE) is an Associate Professor in the Electrical and Computer Engineering Department at Northeastern University. He received a B.S. degree (summa cum laude) in Electrical Engineering from The University of Texas at Arlington in 2003 as well as the M.S. and Ph.D. degrees in Electrical Engineering from Texas A&M University in 2007 and 2011, respectively.

From 2004 to 2005, he was Electrical Test/Product Engineer at Intel Corp. in Hillsboro, Oregon. He joined the Analog and Mixed-Signal Center at Texas

A&M University in 2005, where he was engaged in research projects involving analog built-in testing, data converters, and on-chip temperature sensors for thermal monitoring. In the spring 2011 semester, he worked as a Design Engineering Intern in the Broadband RF/Tuner Development group at Broadcom Corp. in Irvine, California. Marvin Onabajo has been at Northeastern University since the Fall 2011 semester. His research areas are analog/RF integrated circuit design, on-chip built-in testing and calibration, mixed-signal integrated circuits for medical applications, data converters, and on-chip sensors for thermal monitoring. He served as an Associate Editor on the editorial boards of the IEEE Transactions on Circuits and Systems I (TCAS-I) and the IEEE Circuits and Systems Magazine during the 2016-2017, 2018-2019, 2020-2021 and 2022-2023 terms. In 2014 and 2015, he was on the editorial board of the IEEE Transactions on Circuits and Systems II (TCAS-II). He received a 2015 CAREER Award from the National Science Foundation, a 2017 Young Investigator Program Award from the Army Research Office (ARO), as well as the 2015 Martin Essigman Outstanding Teaching Award and the 2022 Faculty Fellow Award from the College of Engineering at Northeastern University.



Francesco Restuccia [M'16, SM'21] is an Assistant Professor in the Department of Electrical and Computer Engineering at Northeastern University. He received his Ph.D. in Computer Science from Missouri University of Science and Technology in 2016, and his B.S. and M.S. in Computer Engineering with highest honors from the University of Pisa, Italy in 2009 and 2011, respectively. His research interests lie in the design and experimental evaluation of next-generation edge-assisted data-driven wireless systems. Prof. Restuccia's research is funded by sev-

eral grants from the US National Science Foundation and the Department of Defense. He received the Office of Naval Research Young Investigator Award, the Air Force Office of Scientific Research Young Investigator Award and the Mario Gerla Award in Computer Science, as well as best paper awards at IEEE INFOCOM and IEEE WOWMOM. Prof. Restuccia has published over 60 papers in top-tier venues in computer networking, as well as co-authoring 16+U.S. patents and three book chapters. He regularly serves as a TPC member and reviewer for several top-tier ACM and IEEE conferences and journals.



Aatmesh Shrivastava (S'12–M'15–SM'19) received his Ph.D. degree from the University of Virginia in 2014. Prior to his Ph.D., he worked as a senior design engineer at Texas Instruments, Bangalore from 2006 to 2010. From 2014 to 2016, he worked at an IoT start-up Everactive as a senior design director, where he was responsible for the research and development of the energy harvesting and power management solutions. In August 2016, he joined Northeastern University, where he is now working as an Associate Professor in the Electrical

and Computer Engineering Department. His research interests include self-powered and ultra-low power circuits and system, energy-harvesting and power-first system/computer architecture, analog computing, internet-of-things (IoT), ultra-low power bio-medical and neural circuits, exa-scale computing, and hardware security. He served as an Associate Editor on the editorial board of the IEEE Transactions on Circuits and Systems Part I: Regular Papers (TCAS-I) from 2023-2024. He currently serves as an Associate Editor on the editorial board of IEEE Open Journal on Circuits and Systems (OJCAS) and as a Senior Editor for the IEEE Journal on Emerging and Selected Topics in Circuits and Systems (JETCAS). He was a recipient of DARPA Young Faculty Award in 2023, NSF CAREER Award in 2022, Acorn Innovation Award from Mass Ventures in 2021, and the 2024 Faculty Fellow Award from the College of Engineering at Northeastern University